Numerical investigation of the vertical plunging force of a spherical intruder into a granular bed

NUMERICAL INVESTIGATION OF THE VERTICAL PLUNGING FORCE OF A SPHERICAL INTRUDER INTO A PREFLUIDIZED GRANULAR BED

Y.(Yupeng) XU[1*], J.T.(Johan) PADDING[1†], M.A.(Martin) VAN DER HOEF[2‡], J.A.M.(Hans) KUIPERS[1§]

[1]Department of Chemical Engineering and Chemistry, Eindhoven University of Technology, 5600 MB, Eindhoven, The Netherlands

[2]Department of Science and Technology, University of Twente, 7500 AE, Enschede, The Netherlands

[*] E-mail: y.xu@tue.nl
[†] E-mail: j.t.padding@tue.nl
[‡] E-mail: m.a.vanderhoef@utwente.nl
[§] E-mail: j.a.m.kuipers@tue.nl

ABSTRACT

The plunging of a large sphere into a prefluidized granular bed with various constant velocities is investigated using a state-of-the-art hybrid Discrete Particle and Immersed Boundary Method (DP-IBM), with which both the gas-induced drag force and the contact force exerted on the intruder can be investigated separately. Our simulation method has been validated by comparison with the existing experimental results. Current simulation results show a concave-to-convex plunging force as a function of depth and in the concave region the force fits to a power-law with exponent around 1.3, which is in good agreement with existing experimental observations.

Keywords: prefluidized granular bed, plunging force, moving internals, Immersed Boundary Method.

NOMENCLATURE

Greek Symbols

ε	Gas volume fraction, $[-]$
η	Dynamic viscosity, $[Pa \cdot s]$
μ	Friction coefficient, $[-]$
ρ	Mass density, $[kg/m^3]$
τ	Viscous stress tensor, $[Pa]$
ω	Angular velocity, $[rad/s]$

Latin Symbols

d	Granular particle diameter, $[m]$
D	Intruder particle diameter, $[m]$
$\mathbf{F}$	Force, $[N]$.
I	Moment of inertia, $[kg \cdot m^2]$.
m	Mass, $[kg]$.
$\mathbf{r}$	Coordinate, $[m]$.
R	Particle radius, $[-]$
$\mathbf{s}$	Force density, $[N/m^3]$
$\mathbf{T}$	Torque, $[N \cdot m]$.
u	Gas velocity, $[m/s]$
v	Particle velocity, $[m/s]$
z	Depth from surface, $[m]$.

Sub/superscripts

a	Particle index a.
b	Particle index b.
c	Contact.
d	Drag.
g	Gas or gravity.
m	Marker-point index.
n	Normal direction.
p	Pressure.
t	Tangential direction.

INTRODUCTION

The plunging of a high-speed intruder into a dense granular bed occurs in many different cases, such as meteor impacts and footprints on sand. Many studies have tried to find the macroscopic force law exerted on the intruder and different variations of the force law were found.

Experimental results (Hou *et al.*, 2005; Katsuragi and Durian, 2007) of a vertically free falling object impacting onto a horizontal bed of granular particles with relatively large initial contact velocities show that the macroscopic force law contains a term scaling as kz, where z is the depth from the surface. In (Hou *et al.*, 2005), hollow cenospheres (diameter $\approx$ 74 - 100 μm) of density 0.693 g/cm^3 are used. Particles are first poured into the bed and then loosed by slowly pulling a sieve (mesh size=0.4 mm) which was initially buried at the bottom. The volume fraction of the bed produced by this procedure consistently gives a value of about 0.54. In (Katsuragi and Durian, 2007), spherical glass beads (diameter range 250-350 μm, density ρ_g = 1.52 g cm^{-3} and friction coefficient $\mu = 0.45$) were used as granular medium. The medium was fluidized, and gradually defluidized by a uniform upflow of N_2 gas. The volume fraction occupied by the beads was 0.590 ± 0.004 after fluidization. A steel sphere of diameter $D = 2.54$ cm was used as a projectile. Also, investigations done by Lohse et al. (Lohse *et al.*, 2004) showed that for freely falling projectiles with zero impact velocity (v_0=0), the macroscopic force law can be described simply by the term kz, where the parameter k characterizes the increase in force with increasing depth z.

Completely different results are obtained for intruders moving with constant but relatively small vertical velocities. Stone et al. pushed a flat plate vertically into a granular medium (Stone *et al.*, 2004a,b), and found that the penetration force increases with increasing depth nearly linearly in an initial regime, then followed by a depth-independent regime. When the plate was pushed near the bottom of the container, the penetration force showed an exponential increase. The authors deem that the initial linear regime is due to hydrostatics while the depth-independent regime is a Janssen-like regime, which is due to side wall support. Hill

et al.(Hill *et al.*, 2007) measured the drag force of an intruder plunging into and withdrawing from a shallow granular bed (about 100 mm), and found that both the plunging and the withdrawing forces had power-law dependence on the immersion depth with exponents greater than unity, i.e., 1.3 for plunging and 1.8 for withdrawing. Peng et al. (Peng *et al.*, 2009) found that the plunging force curves of fully immersed intruders have a concave-to-convex transition and the depth dependence of the force turns from supralinear to sublinear. They found that the plunging force at the inflection point is proportional to the intruder's volume and the inflection point occurs when the intruder is fully buried to a level of around twice its diameter. Within the shallow regime, i.e. before reaching the inflection point, the plunging force fits exhibits a power-law dependence for all spherical intruders, with an exponent of 1.3 ± 0.02.

Clearly, the form of the force experienced by an impacting intruder is still not unified, and understanding of this problem remains limited. At the same time, we are also interested in the details of this plunging process, such as the reorganization of the granular particles around the large intruder. Simulations are an effective alternative way to investigate this problem. In our former work, a state-of-the-art discrete particle method (DPM) combined with an immersed boundary (IB) method was introduced to investigate the kinematics of an intruder freely dropping on a prefluidized granular bed. We showed that our simulations results are in good agreement with the experimental observations, thus offers another powerful tool to investigate the gas-induced and contact forces directly and independently (Xu *et al.*, 2013).

According to former experimental results, the granular plunging process is influenced by many parameters, such as the intruder diameter D, plunging depth z, and intruder velocity v. Thus, a very straightforward idea would be to vary one parameter whilst keeping the other parameters constant. In this paper, we use our simulation method to further investigate the force on an intruder moving with a constant velocity through a prefluidized bed. The relation between the force F and the intruder penetration depth z, intruder diameter D, and intruder velocity v are investigated. Moreover, the re-arrangement of the granular particles in the bed is investigated by using a layer colored bed.

MODEL DESCRIPTION

The DPM-IBM model used in this work has been detailed in another work (Xu *et al.*, 2013) and the applicability of the model has been verified by a good agreement between the our simulation results and existing experimental work. Our model consists of two major sub-models, the discrete particle (DP) and immersed boundary (IB) model. The DP model deals with the motion of suspended small (granular) particles, taking into account the action of gravity, gas-solid drag forces, as well as particle-particle and particle-wall collisions. In this model, the gas phase is solved on a computational mesh with a length scale larger than the size of the small particles and the gas-particle coupling is treated by empirical drag relations (Van der Hoef *et al.*, 2006). The IB method deals with the motion of the large intruder through the continuous phase (consisting of gas and suspended solid particles).

We now give a brief technical description of the DP model and the IB method. A schematic representation of the DP model and IB method is shown in figure 1.

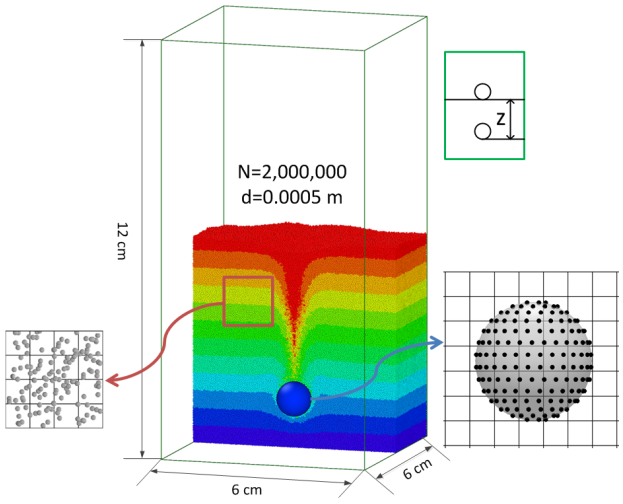

Figure 1: Schematic representation of the DP and IB methods. In the DP model the motion of the small particles is solved, taking into account detailed contact forces, as well as drag forces caused by motion relative to the interstitial gas. The particles are smaller than the grid on which the gas phase equations are solved (left), requiring empirical drag relations. The intruder is much larger than the gas grid and coupled to the gas phase through the IB method, which enforces no-slip boundary conditions by a distribution of force points across the surface of the intruder (right). Schematic representation of (half) the bed geometry is also shown (center); particles are colour coded according to their initial position in z direction. Visualization was carried out using OVITO (Stukowski, 2009).

Equations of motion for the small particles

The motion of a spherical granular particle a with mass m_a, moment of inertia I_a and coordinate $\mathbf{r}_a$ is described by Newton's equations for rigid body motion:

$$m_a \frac{\mathrm{d}^2 \mathbf{r}_a}{\mathrm{d}t^2} = \mathbf{F}_{\mathrm{g},a} + \mathbf{F}_{\mathrm{d},a} + \mathbf{F}_{\mathrm{p},a} + \mathbf{F}_{\mathrm{c},a} \qquad (1)$$

$$I_a \frac{\mathrm{d}\boldsymbol{\omega}_a}{\mathrm{d}t} = \mathbf{T}_a \qquad (2)$$

The four terms on the right-hand side of Eq 1 account for the gravitational force, the gas drag force, the force due to pressure gradients in the gas phase, and the sum of the individual contact forces exerted by all other particles in contact with particle a. In Eq 2 , $\boldsymbol{\omega}_a$ is the angular velocity and $\mathbf{T}_a$ is the torque around the centre-of-mass of particle a. Regarding the contact model, two types of collision models are widely used, namely the hard sphere model and the soft sphere model. In our simulation, the soft sphere model is used since the hard sphere model is not suited for systems where quasi static particle configurations exist. More detailed information can be found in (Van der Hoef *et al.*, 2006; Alder and Wainwright, 1957).

For the calculation of $\mathbf{F}_{\mathrm{c},a}$, a three-dimensional linear spring and dashpot type soft sphere collision model along the lines of Cundall and Strack is used (Cundall and Strack, 1979; van Sint Annaland *et al.*, 2005; Xiong *et al.*, 2011). In this model, the total contact force on particle a of radius R_a is given by a

sum of normal and tangential pair forces with neighbouring particles,

$$\mathbf{F}_{\mathrm{c},a} = \sum_{b \in \text{contactlist}} (\mathbf{F}_{n,ab} + \mathbf{F}_{t,ab}) \tag{3}$$

where the normal forces $\mathbf{F}_{n,ab}$ depend linearly on the overlap $\delta = R_a + R_b - |\mathbf{r}_a - \mathbf{r}_b|$ and the relative normal velocity $\mathbf{v}_{n,ab} = ((\mathbf{v}_a - \mathbf{v}_b) \cdot \mathbf{n}_{ab})\,\mathbf{n}_{ab}$, with $\mathbf{n}_{ab}$ the unit vector pointing from the centre of b to the centre of a. Similarly, the tangential forces $\mathbf{F}_{t,ab}$ depend linearly on the tangential overlap δ_t, defined as the integral of the relative tangential velocity from the time of first contact, and the relative tangential velocity $\mathbf{v}_{t,ab} = (\mathbf{v}_a - \mathbf{v}_b) - \mathbf{v}_{n,ab}$ itself. The tangential forces also lead to a torque on the particles:

$$\mathbf{T}_a = \sum_{b \in \text{contactlist}} (R_a \mathbf{n}_{ab} \times \mathbf{F}_{t,ab}) \tag{4}$$

Governing equations for the gas phase

The gas flow is governed by the conservation equations for mass and momentum:

$$\frac{\partial(\varepsilon\rho_g)}{\partial t} + \bigtriangledown \cdot \varepsilon\rho_g \mathbf{u} = 0 \tag{5}$$

$$\frac{\partial(\varepsilon\rho_g \mathbf{u})}{\partial t} + \bigtriangledown \cdot \varepsilon\rho_g \mathbf{u}\mathbf{u} = -\varepsilon \bigtriangledown p - \bigtriangledown \cdot \varepsilon\tau + \varepsilon\rho_g \mathbf{g} \tag{6}$$

$$+\mathbf{s}_p + \mathbf{s}_{\mathrm{ibm}}, \tag{7}$$

where ε is the local gas voidage (gas volume fraction), ρ_g is the gas phase density, $\mathbf{u}$ the gas velocity, p the gas pressure, τ the viscous stress tensor, $\mathbf{g}$ the gravitational acceleration, $\mathbf{s}_{\mathrm{ibm}}$ the source term for the momentum exchange with large bodies such as an intruder, and $\mathbf{s}_p$ a source term which describes the momentum exchange with the small solid particles:

$$\mathbf{s}_p = \sum_{a=1}^{N_{\mathrm{part}}} \mathbf{F}_{\mathrm{d},a}\,\delta(\mathbf{r} - \mathbf{r}_a) \tag{8}$$

where the summation is performed over all particles and the drag force $\mathbf{F}_{\mathrm{d},a}$ is identical to what is used in the equation of motion of the particles. For the momentum exchange with small solid particles which are smaller than the Eulerian grid, it is necessary to introduce empirical drag correlations to take the gas-particle interaction into account:

$$\mathbf{F}_{\mathrm{d},a} = 6\pi\eta_g R_a (\mathbf{u} - \mathbf{v}_a) \cdot \mathrm{F}(\mathrm{Re}, \varepsilon) \tag{9}$$

where η_g is the dynamic gas viscosity. For $\mathrm{F}(\mathrm{Re}, \varepsilon)$ the Ergun (Ergun, 1952) and Wen&Yu (Wen and Yu, 1966) correlations are used:

$$\mathrm{F}(\mathrm{Re}, \varepsilon) = \begin{cases} \varepsilon^{-2.65}(1 + 0.15\mathrm{Re}^{0.687}) & \text{for} \quad \varepsilon > 0.8 \\ \dfrac{150}{18}\dfrac{1-\varepsilon}{\varepsilon} + \dfrac{1.75}{18}\dfrac{\mathrm{Re}}{\varepsilon} & \text{for} \quad \varepsilon < 0.8 \end{cases} \tag{10}$$

here $\mathrm{Re} = 2R_a\rho_g\varepsilon|\mathbf{u} - \mathbf{v}_a|/\eta_g$ is the particle Reynolds number.

Immersed boundary method

The interaction of the gas phase with an intruder larger than the size of the CFD cells is modelled with the immersed boundary method (IBM) where Lagrangian marker points are situated on the boundary of the large particle. Each marker exerts a force on the gas phase such that the local velocity of the gas is equal to the velocity of that marker. IBM has been widely used to study fluid-structure interaction and was pioneered by Peskin to investigate cardiac flow problems (Peskin, 2002). Subsequently, the method has been extended to flow around rigid bodies. The implementation that we adopt is along the lines of Uhlmann (Uhlmann, 2005). The IBM source term $\mathbf{s}_{\mathrm{ibm}}$ at the grid cell faces is calculated by summing the contribution of all Lagrangian force points:

$$\mathbf{s}_{\mathrm{ibm}} = \sum_{m=1}^{N_{\mathrm{langr}}} \mathbf{F}_m\,\delta(\mathbf{r} - \mathbf{r}_m), \tag{11}$$

where in our discretised simulations $\mathbf{F}_m$ is constructed such that the forcing results in a zero slip velocity at the surface of the sphere and $\delta(\mathbf{r} - \mathbf{r}_m)$ is a volume weighing delta function which distributes the forces to the surrounding grid cell faces. For detailed implementation of this method we refer to (Deen *et al.*, 2004; Gerner, 2009; Kriebitzsch, 2011).

Table 1: Parameters used in the simulations

Gravity z-direction	$\mathrm{m/s^2}$	9.81
Intruder diameter	m	0.01
Intruder density	$\mathrm{kg/m^3}$	2500
Particle diameter	m	5×10^{-4}
Particle density	$\mathrm{kg/m^3}$	2500
Restitution coefficient (normal)	–	0.97
Restitution coefficient (tangential)	–	0.33
Friction coefficient	–	0.10
Normal spring stiffness	N/m	100
Tangential spring stiffness	N/m	32.13
Contact time step	s	7.2×10^{-5}
Gas viscosity	kg/(ms)	1.8×10^{-5}
Computation domain		
x-direction	m	0.06
y-direction	m	0.06
z-direction	m	0.12
Number of grid cells		
x-direction	–	30
y-direction	–	30
z-direction	–	60

SIMULATION SETTINGS

In the simulation, we use a container with dimensions $6 \times 6 \times 12$ $\mathrm{cm^3}$ (width, depth, height). It contains one large intruder and 2,000,000 granular particles. The intruder has a diameter of 1 cm, while the granular particles are of average diameter 0.5 mm, with a Gaussian size distribution ($\sigma = 0.02$ mm) to avoid excessive ordering of the bed. According to the experimental results shown in (Nelson *et al.*, 2008) and (Seguin *et al.*, 2008), the ratio between size of the container and the intruder in our simulation ($L_{box}/D = 6$) is large enough so that the surrounding walls have negligible effect on the dynamics of the intruder. A schematic representation of the bed geometry is shown in figure 1. A summary of the simulation parameters is given in table 1.

In all simulations the coefficient of restitution is set to 0.97 for the normal direction, and to 0.33 for the tangential direction. For the particle-wall interaction the same collision parameters are used as for the particle-particle interaction. The friction coefficient is set to 0.1. All these values are typical for glass spheres/walls. We note that the normal spring stiffness k_n is in principle related to Young's modulus and the

Poisson ratio of the solid material; however, in practice its value must be chosen much smaller to prevent the use of impractically small integration time steps. Therefore the spring stiffness is chosen as low as possible while ensuring that the lowered spring stiffness does not have a significant influence on the phenomena observed. We investigated the influence of varying the spring stiffness between $k_n = 100, 200, 400$ and 800 N/m with an intruder initially located at z = 0.11 m and initial velocity equal to 2 m/s. The results showed that the lower normal stiffnesses do not significantly influence the collision kinematics (not shown). Thus, to enhance the computational efficiency, $k_n = 100$ N/m was used in all subsequent simulations. The granular particles are fluidized by a uniform up-flowing gas, which was gradually turned off with the goal to make a homogeneous particle bed with a flat surface. The depth of the resulting static bed is about 5.84 cm with a solids volume fraction of about 0.62. For most simulations reported here, we let the intruder move constantly downwards from a height of 11 cm, which is about 5 cm above the bed and stop near the bottom. The only exception is the validation of the model reported in the next section, where we apply a constant external gravitational force on the intruder.

VALIDATION

The validation of our simulations is done by comparing our simulation results with the experimental work by Katsuragi and Durian (Katsuragi and Durian, 2007). Unfortunately, a full one-to-one comparison is not possible due to limitations in computing capacity. That is, our granular particles are about two times larger while the intruder is 2.5 times smaller than the experimental ones.

The complete data sets for the position $z(t)$, velocity $v(t)$, and acceleration $a(t) + g$ of the intruder are shown in figure 2. The time origin is *defined* as the time of initial impact, and the position is measured upwards from the granular surface, opposite to the gravitational direction. The curves are colour-coded according to the initial impact speed of the intruder, v_0, which ranges from 0 to 400 cm/s, similar to the values used by Katsuragi and Durian (Katsuragi and Durian, 2007). Although a quantitative agreement is not expected because of the different particle diameters, the observed time evolution of the intruder dynamics is in good qualitative agreement with the experimental results, which are repeated here also for clarity. More details can be found in our previous work (Xu *et al.*, 2013) which shows that also other measurements, such as oscillatory terminal behaviour and the dependence of the final penetration depth on impact velocity, are in good agreement with experimental observations.

RESULTS

In these new simulations, the intruder is moved at constant velocity through the granular bed. Because the time step needs to be small in order to successfully capture the details of the collision processes, the simulation time for extremely small intruder velocities would become prohibitively long. Thus in the current simulations, the lowest intruder velocity was limited to 0.01 m/s. According to Albert et al. (Albert *et al.*, 1999), when the velocity of the intruder is less than $v < \sqrt{2gd}/10 \approx 0.01$ m/s, the system is in the so-called low velocity regime where the force exerted on the intruder is independent of the plunging velocity. On the other hand, due to the limited size of the system, boundary effects are expected to become important at very large velocities. Also by checking the animation, we found that for larger intruder velocities, a long channel following the intruder will form and will take more time to be refilled by granular particles. We therefore limited our intruder velocity to a maximum of 0.40 m/s.

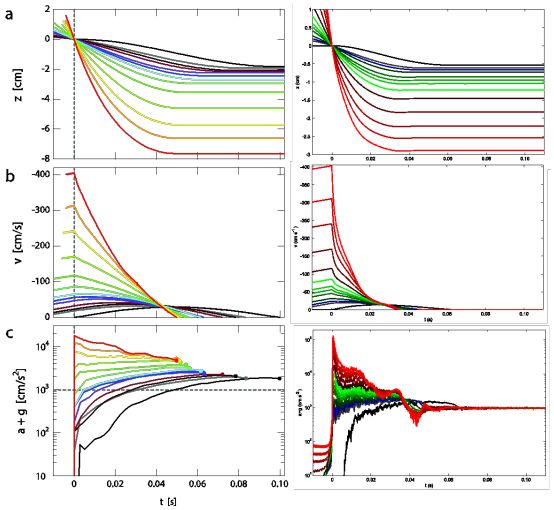

Figure 2: Detailed comparison between literature results (left) and our simulation results (right) for (a) the intruder depth, (b) intruder speed and, (c) net acceleration versus time for an intruder driven by gravity. Reproduced with permission from (Katsuragi and Durian, 2007). Note that the granular particle size is about two times smaller and the intruder 2.5 times larger than in our simulations. Curves are colour-coded according to the initial impact speed of the intruder, v_0, which can be read from panel (b) at $t = 0$.

Figure 3 shows snapshots of the bed configuration at the time when a $D = 10$ mm spherical intruder has moved one diameter ($z = D$) since initial contact, at four different impact velocities of $v_0 = 0.1$, 0.2, 0.3 and 0.4 m/s. Note how the granular particles are perturbed much more at higher velocities, leading to formation of a granular crater. Investigation of the force experienced by an intruder moving at constant velocity is very helpful to understand the dynamics of granular cratering and the factors that determine its severity. Because both the plunging velocity and the intruder size are important parameters, we investigate them separately.

Figure 4 shows the force experienced by the 10 mm spherical intruder under different impact velocities. At the low-

Figure 3: Bed structure under different impact velocities of a 10 mm spherical intruder at the time when the intruder has moved one diameter since initial contact. Granular particles are colour coded according to their velocities.

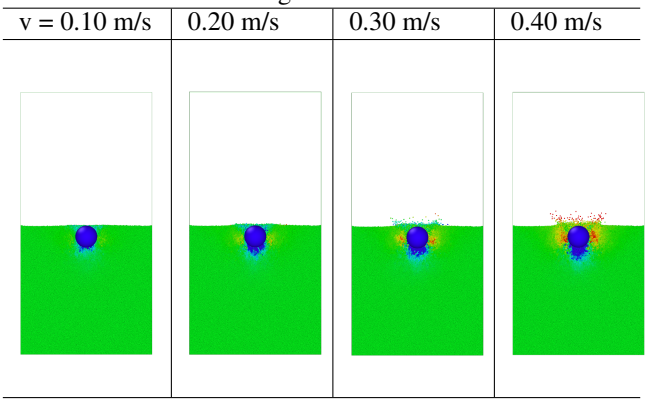

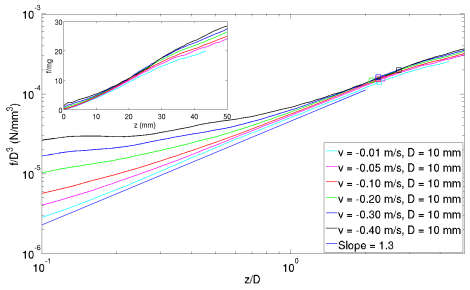

Figure 4: Plunging force f of a 10 mm intruder with different intruding velocities as a function of penetration depth z. The inset shows the measured force on the intruder, nondimensionalised by its weight, on a linear scale. The main plot shows the measured force on a double-logarithmic scale, emphasizing its power-law dependence. The inflection point is indicated by a square on each curve.

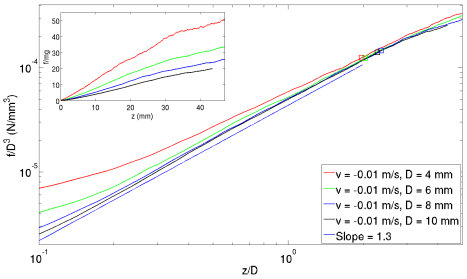

Figure 5: Plunging force f of intruders with different size under an impact velocity of 0.1 m/s as a function of penetration depth z. The inset shows the measured force on the intruder, nondimensionalised by its weight, on a linear scale. The main plot shows the measured force nondimensionalised by the intruder volume D^3 versus penetration depth nondimensionalised by the intruder diameter D, both on a logarithmic scale. The inflection point is indicated by a square on each curve.

est intruder velocity of 0.01 m/s, we find a good agreement with a total force scaling as a power-law with exponent 1.3, up to a depth of slightly more than twice the intruder diameter D. For higher intruder velocities, the initial force is slightly larger, but converges to the same power-law behaviour beyond a depth of approximately one intruder diameter. Moreover, a concave-to-convex transition it observed at all intruder velocities. These results are very similar to the former experimental results in (Peng *et al.*, 2009; Hill *et al.*, 2007). It was found that, in the experiments, the inflection point occurs when the intruder is fully buried to a level of 2.4 times the intruder diameter. In our simulations, the inflection point occurs similarly at a depth ranging from 2.0 to 2.7 times the intruder diameter, as shown in figures 4 and 5. Note that for high intruder velocities the impact is relatively violent and the forces exerted on the intruder are quite noisy. Thus for velocities larger than 0.10 m/s, forces have been averaged over different runs. Further smoothing using an averaging window of 2.5 mm was applied for all velocities.

Figure 5 shows the force experienced by spherical intruders of different size, ranging from $D = 4$ mm to 10 mm, at an impact velocity of 0.1 m/s. When we scale the penetration depth z by the intruder diameter D, and scale the force f by D^3, as conducted in (Peng *et al.*, 2009), all the data collapses for depths beyond approximately D. A slight offset is observed for different intruder diameters, which is related to different velocity-dependent drag forces experienced by the intruders. This is the topic of ongoing work which will be reported in a future paper.

CONCLUSION

A state-of-the-art DPM-IBM model has been extended to study the vertical plunging force of a spherical intruder into a granular bed. Our simulation method has been validated by our former work (Xu *et al.*, 2013) on gravity-driven intruder dynamics. In the current work we used it to investigate the force on the intruder when it is inserted into the granular bed at constant velocity. Our method successfully captures the experimentally observed concave-to-convex plunging force behaviour. In the initial regime, we find that the force fits to a power-law with an exponent of 1.3, which is also in good agreement with existing experimental observations. Finally, the plunging force for different intruder diameters is observed to approach a master curve when the force is scaled with the intruder volume and the pentration depth is scaled with the intruder diameter. The deviations are mainly a consequence of differences in the drag force experienced by the intruder, which is a topic of future work.

ACKNOWLEDGEMENTS

This work is part of the research program of the Foundation for Fundamental Research on Matter (FOM), which is part of the Netherlands Organization for Scientific Research (NWO).

REFERENCES

ALBERT, R. *et al.* (1999). "Slow drag in a granular medium". *Physical review letters*, **82(1)**, 205–208.

ALDER, B. and WAINWRIGHT, T. (1957). "Phase transition for a hard sphere system". *The Journal of Chemical Physics*, **27(5)**, 1208–1209.

CUNDALL, P.A. and STRACK, O.D. (1979). "A discrete numerical model for granular assemblies". *Geotechnique*, **29(1)**, 47–65.

DEEN, N.G. *et al.* (2004). "Multi-scale modeling of dispersed gas–liquid two-phase flow". *Chemical Engineering Science*, **59(8)**, 1853–1861.

ERGUN, S. (1952). "Fluid flow through packed columns". *Chem. Eng. Prog.*, **48**, 89–94.

GERNER, H.J. (2009). *Newton vs Stokes: Competing Forces in Granular Matter*. University of Twente.

HILL, G. *et al.* (2007). "Scaling vertical drag forces in granular media". *EPL (Europhysics Letters)*, **72(1)**, 137.

HOU, M. *et al.* (2005). "Projectile impact and penetration in loose granular bed". *Science and Technology of Advanced Materials*, **6(7)**, 855–859.

KATSURAGI, H. and DURIAN, D. (2007). "Unified force law for granular impact cratering". *Nature Physics*, **3(6)**, 420–423.

KRIEBITZSCH, S.H. (2011). *Direct Numerical Simulation of Dense Gas-Solid Flows*. Eindhoven University of Technology.

LOHSE, D. *et al.* (2004). "Granular physics: creating a dry variety of quicksand". *Nature*, **432(7018)**, 689–690.

NELSON, E.L. *et al.* (2008). "Projectile interactions in granular impact cratering". *Phys. Rev. Lett.*, **101**, 068001.

PENG, Z. *et al.* (2009). "Depth dependence of verti-

cal plunging force in granular medium". *Phys. Rev. E*, **80**, 021301.

PESKIN, C.S. (2002). "The immersed boundary method". *Acta numerica*, **11(0)**, 479–517.

SEGUIN, A. *et al.* (2008). "Influence of confinement on granular penetration by impact". *Phys. Rev. E*, **78**, 010301.

STONE, M.B. *et al.* (2004b). "Local jamming via penetration of a granular medium". *Phys. Rev. E*, **70**, 041301.

STONE, M.B. *et al.* (2004a). "Stress propagation: Getting to the bottom of a granular medium". *Nature*, **427(6974)**, 503–504.

STUKOWSKI, A. (2009). "Visualization and analysis of atomistic simulation data with ovito–the open visualization tool". *Modelling and Simulation in Materials Science and Engineering*, **18(1)**, 015012.

UHLMANN, M. (2005). "An immersed boundary method with direct forcing for the simulation of particulate flows". *Journal of Computational Physics*, **209(2)**, 448–476.

VAN DER HOEF, M. *et al.* (2006). "Multiscale modeling of gas-fluidized beds". *Advances in chemical engineering*, **31**, 65–149.

VAN SINT ANNALAND, M. *et al.* (2005). "Numerical simulation of gas–liquid–solid flows using a combined front tracking and discrete particle method". *Chemical engineering science*, **60(22)**, 6188–6198.

WEN, C. and YU, Y. (1966). "Mechanics of fluidization". *Chem. Eng. Prog. Symp. Ser.*, vol. 62, 100.

XIONG, Q. *et al.* (2011). "Large-scale dns of gas-solid flows on< i> mole-8.5</i>". *Chemical Engineering Science*.

XU, Y. *et al.* (2013). "Detailed numerical simulation of an intruder impacting on a granular bed using a hybrid discrete particle and immersed boundary (dp-ib) method". *Chemical Engineering Science*, **104**, 201–207.